20. Core samples were maintained at −70°C until ultrasonically extracted with 2:1 CH$_3$OH/CH$_2$Cl$_2$ in an ice bath. Total lipid extracts were separated by silica gel column chromatography into hydrocarbon, diglyceride, and phospholipid fractions. PLFAs were transesterified with NaOCH$_3$ to methyl esters. PLFA quantification and structural confirmations were achieved by gas chromatography and mass spectrometry with octacosanoic acid methyl ester as an internal standard. PLFA stable-carbon isotopic compositions were determined by gas chromatography and isotope ratio monitoring mass spectrometry. ^{13}C data are reported with δ^{13}C notation as ‰ deviation from the Pee Dee Belemnite standard and were corrected for the addition of methyl carbon during transesterification.
21. Growth medium contained 7.5 mM Na$_2$PO$_4$, 5.9 mM KH$_2$PO$_4$, 0.8 mM MgSO$_4$, 15 mM (NH$_3$)$_2$SO$_4$, and HCl (to pH 3).
22. Shale substrate was prepared by powdering, autoclaving, and ultrasonically extracting unweathered New Albany Shale (6.8% C$_{org}$, 3.2% FeS$_2$) in 2:1 CH$_2$Cl$_2$/CH$_3$OH. The extracted shale was then dried at 40°C for 18 hours to drive off solvent.
23. To monitor cells, 2 to 10 μl were removed from cultures and either dried in air onto microscope slides or filtered onto black polycarbonate membranes (0.2 μm). Slides and filters were stained with DAPI (4′,6′-diamidino-2-phenylindole), which binds to DNA, or acridine orange, which binds to DNA and RNA. Slides and mounted filters were observed with a Zeiss Axiovert S100 equipped with a Hg vapor lamp.
24. Inoculum (200 μl) was added to 10 ml of growth medium and 1 g of shale substrate. Additional substrate and medium were added over 10 days to a final volume of 200 ml of medium and 40 g of shale. The culture was incubated at 25°C in the dark until harvested for PLFA analysis. Total DAPI-stained microbial population immediately before harvesting was ~10^8 cells/ml, extrapolated from 20 counts conducted on three separate filters.
25. The culture was centrifuged to separate solids from growth medium, and then extracted as in (*20*).
26. PFLA methyl esters from the culture were separated by preparative scale gas chromatography into four PLFA compound classes. Purified PLFAs were sealed in evacuated quartz tubes with CuO and combusted to CO$_2$ at 850°C. CO$_2$ was reduced to graphite targets over a Co catalyst and analyzed for ^{14}C content by the National Ocean Science Mass Spectrometry facility at Woods Hole Oceanographic Institution.
27. P. Nielsen, S. O. Petersen, *Soil Biol. Biochem.* **32**, 1241 (2000).
28. R. H. Findlay, M. B. Trexler, J. B. Guckert, D. C. White, *Mar. Ecol. Prog. Ser.* **62**, 121 (1990).
29. N. J. E. Dowling, F. Widdel, D. C. White. *J. Gen. Microbiol.* **132**, 1815 (1986).
30. R. J. Parkes, J. Taylor, *Estuar. Coast. Shelf Sci.* **16**, 173 (1983).
31. Fluorescent in situ hybridizations were performed on core samples and cultures with established hybridization protocols and fluorescent-labeled probes (universal and domain-level bacterial, archaeal, and eukaryotic probes). Positive hybridizations and negative controls showed that in culture and deepest core samples, the cell population was predominantly Bacteria, with smaller numbers of Archaea and Eukarya.
32. Carbonate-free shale was prepared by digesting powdered, solvent-extracted shale in 12 M HCl at 25°C with stirring for 24 hours, followed by multiple washes in an excess of distilled water until the pH of washes reached 5. Kerogen was isolated from carbonate-free shale by digestion in 48% HF at 25°C for 18 hours in Teflon centrifuge tubes. HF-digested shale was rinsed in an excess of distilled water, then suspended in a 60% ZnBr$_2$ solution (density, 1.6 g/cm^3) and centrifuged at 4500 rpm for 30 min to separate pyrite from OM. Floated material was collected; rinsed in distilled H$_2$O, CH$_3$OH, and CH$_2$Cl$_2$; and dried at 40°C to remove solvent.
33. Polished blocks of unweathered New Albany Shale were sterilized by autoclaving at 120°C for 20 min, and then introduced into existing cultures. Blocks were removed after 24, 48, and 96 hours. Blocks were rinsed in sterile growth medium to remove loosely attached cells, stained with acridine orange, and viewed by epifluorescence microscopy to examine attachment of microbial cells to the shale surface.
34. H. T. S. Boschker, J. F. C. de Brouwer, T. E. Cappenberg. *Limnol. Oceanogr.* **44**, 309 (1999).
35. R. A. Berner, *Paleogeogr. Paleoclimatol. Paleoecol.* **75**, 97 (1989).
36. S. T. Petsch, R. A. Berner, *Am. J. Sci.* **298**, 246 (1998).
37. R. A. Berner, D. E. Canfield, *Am. J. Sci.* **289**, 333 (1989).
38. R. A. Berner *et al.*, *Science* **287**, 1630 (2000).
39. We thank J. M. Hayes, E. A. Webb, R. A. Berner, and the reviewers for their comments; D. Montluçon and S. Kaufman for field assistance and sample preparation; and A. P. McNichol and D. Stuart (WHOI-NOSAMS) for ^{14}C analyses. Supported by NSF grants EAR-9805517 (T.I.E.) and EAR-87399800 (K.J.E.) and the Woods Hole/USGS Postdoctoral Scholars Program. This is WHOI contribution 10439.

15 December 2000; accepted 20 March 2001
Published online 15 December 2001;
10.1126/science.1058332
Include this information when citing this paper.

Quantum Electronic Stability of Atomically Uniform Films

D.-A. Luh,[1,2] T. Miller,[1,2] J. J. Paggel,[3] M. Y. Chou,[4]
T.-C. Chiang[1,2*]

We have studied the structural stability of thin silver films with thicknesses of $N = 1$ to 15 monolayers, deposited on an Fe(100) substrate. Photoemission spectroscopy results show that films of $N = 1$, 2, and 5 monolayer thicknesses are structurally stable for temperatures above 800 kelvin, whereas films of other thicknesses are unstable and bifurcate into a film with $N \pm 1$ monolayer thicknesses at temperatures around 400 kelvin. The results are in agreement with theoretical predictions that consider the electronic energy of the quantum well associated with a particular film thickness as a significant contribution to the film stability.

Structures and devices of nano-dimensions have useful and possibly unique properties (*1*), and an important issue for practical applications is structural stability. As the physical size of a system approaches atomic dimensions, quantum effects are likely to play a significant role. Here we demonstrate that quantum electronic effects can be the dominant factor for the stability of thin films. We used thin Ag films prepared on Fe(100), which can be made with atomic-layer precision up to ~100 monolayers (ML) and over a macroscopic area (*2*). Angle-resolved photoemission from these films shows quantum-well states corresponding to confined electrons. Cutoff of the occupancy of these states at the Fermi level gives rise to monolayer-by-monolayer variations in total electronic energy. The predicted stability for films with $N > 1$ agrees well with an experiment in which each film is ramped up in temperature until its geometry changes. Films with thicknesses of $N = 1$, 2, and 5 ML are unusually stable, and remain intact to temperatures above 800 K. Other films with thicknesses of N up to 15 begin to evolve at temperatures around 400 K and bifurcate into adjacent-integer-monolayer thicknesses $N \pm 1$. In our experiment, no specific “magic thicknesses” (*3*–*5*) are ultimately produced. Recent work on Au nanowires has concluded that atomic packing is the deciding factor underlying structural stability, and that electronic effects are less important because of the lack of *d*-electron participation at the Fermi level (*6*, *7*). Ag is electronically similar to Au, and the present results constitute a counter example.

To determine the film thickness and its evolution, we used angle-resolved photoemission. Quantum-well states arising from electron confinement in a film have energies uniquely related to the film thickness (*8*, *9*). Photoemission probes these energy levels directly and is thus a sensitive tool for absolute film thickness measurement. Atomically uniform films of Ag of thicknesses $N = 1$ to 15 were prepared, and the temperature of each film was then ramped up slowly from a base temperature of ~110 K (also the initial Ag deposition temperature), while spectra were taken repetitively to monitor any spectral changes. Results for initial film thicknesses of 6 and 3 ML (Fig. 1) illustrate the general behavior. The spectra taken at low temperatures (top spectrum in each panel) show

---

[1] Department of Physics, University of Illinois at Urbana–Champaign, 1110 West Green Street, Urbana, IL 61801–3080, USA. [2] Frederick Seitz Materials Research Laboratory, University of Illinois at Urbana–Champaign, 104 South Goodwin Avenue, Urbana, IL 61801–2902, USA. [3] Freie Universität Berlin, Institut für Experimentalphysik, 14195 Berlin, Germany. [4] School of Physics, Georgia Institute of Technology, Atlanta, GA 30332–0430, USA.

*To whom correspondence should be addressed. E-mail: chiang@mrl.uiuc.edu

Fig. 1. Normal emission spectra of Ag films on Fe(100) with initial thicknesses of 6 ML (**left**) and 3 ML (**right**) taken with a photon energy of 15 eV. The spectra, from top to bottom, were taken at increasingly higher temperatures, with the bottom spectra taken after the sample had cooled. Quantum-well peaks corresponding to various thicknesses are indicated.

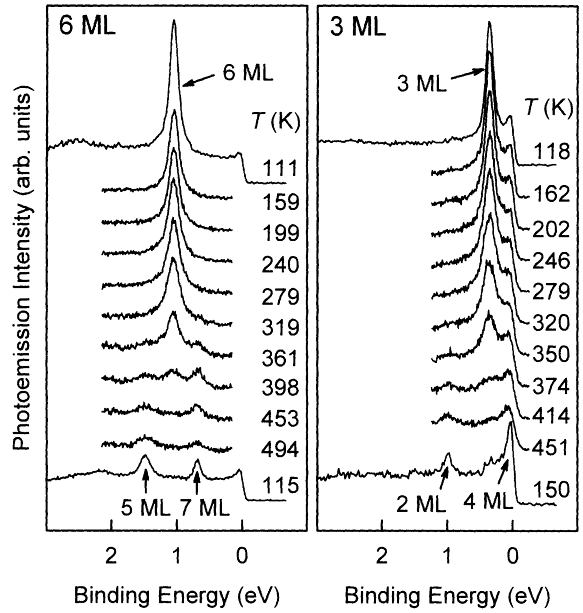

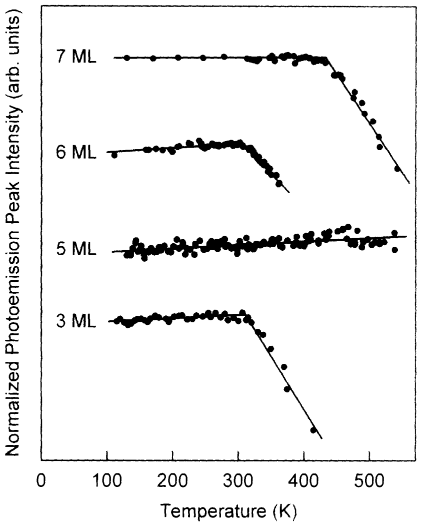

Fig. 2. Quantum-well peak intensities for initial film thicknesses of 3, 5, 6, and 7 ML as a function of sample temperature. Circles are data points, and the line segments are results of linear regression and illustrate the sharp drop-off at the onset of film thickness bifurcation.

sharp quantum-well peaks, whose positions are indicative of the film thicknesses (*8*, *9*). Emission spectra for the 6-ML film show that, as the sample temperature *T* increases, the 6-ML peak begins to broaden thermally (Fig. 1, left). As *T* rises above ~320 K, the peak intensity rapidly decreases, and two new peaks emerge simultaneously. These new quantum-well peaks derive from film thicknesses of 5 and 7 ML. Thus, the original 6-ML film bifurcates into two adjacent-integer-monolayer thicknesses. After the film temperature is increased to more than 500 K, the film is allowed to cool to 115 K (bottom spectrum), and the resulting sample is predominantly a mixture of 6 ± 1 = 5- and 7-ML thicknesses.

The data for an initial film thickness of 3 ML (Fig. 1, right) show a similar behavior. At the end of the heating cycle, the film has mostly bifurcated into a mixture of 3 ± 1 = 2- and 4-ML thicknesses. The relative intensities of the peaks are not necessarily a good indication of the surface area covered by each thickness, because the photoemission cross sections of quantum-well peaks are strongly dependent on the photon energy and film thickness (*10*). The 4-ML peak sits almost exactly on the Fermi level, and its intensity is significantly cut off by the Fermi-Dirac distribution function. All films studied for N up to 15, except for $N = 1$, 2, and 5, bifurcate in a similar manner at temperatures around 400 K. The exceptional cases—$N = 1$, 2, and 5—are much more stable. Films with $N = 5$ are stable up to the highest temperature, 900 K, used in our experiment. The $N = 1$ and 2 films are stable to over 800 K.

The threshold temperature for film instability can be determined by monitoring the photoemission intensity of the quantum-well peak while ramping the sample temperature upward. Examples of such temperature scans (Fig. 2) demonstrate a sharp drop in intensity as the film geometry begins to change. Results from such measurements for N up to 15 are shown in Fig. 3A. The result for the stable film thickness at $N = 5$ represents a lower bound, and the data point is simply the highest temperature that the film has been subjected to. Multiple data points are shown for several thicknesses as an indication of the degree of reproducibility.

Because the electronic states in such films are quantized, there can be considerable monolayer-by-monolayer variation in total electronic energy, depending on where the Fermi level cuts off the occupancy of these states. The quantum-well levels near the Fermi level are exclusively of the free electron–like *sp* character for the Ag films. Their energies E are determined by the bulk band structure and the boundary conditions that are tied to the phase shift function $\Phi(E)$. The relevant equation is the Bohr-Sommerfeld quantization rule (*8*–*10*)

$$2k_z(E)Nt + \Phi(E) = 2n\pi \qquad (1)$$

where k_z is the component of the momentum perpendicular to the film surface, $k_z(E)$ is determined by the band structure, t is the monolayer thickness, and n is a quantum number. To model the present system, we used a realistic band structure based on the combined interpolation scheme (*11*). For simplicity, the 4*d* bands of Ag are removed from the calculation. These bands are located 4 eV below the Fermi level and are fully occupied. An experimentally determined phase-shift function $\Phi(E)$ (*8*) is used, which yields quantum-well state energies at the surface Brillouin zone center in excellent agreement with the experiment.

Equation 1 is easily generalized to quantum-well states with finite k_x and k_y. Each quantum number n is thus associated with a subband (*10*). Such subbands are nearly parabolic near the surface zone center, but the exact dispersions are determined by the band structure and can deviate substantially from nearly-free-electron behavior near the (111) neck of the Ag Fermi surface. Our calculation incorporates the full *sp* band structure, and it would be interesting to explore whether or not the (111) neck, or departure from a spherical Fermi surface, has an important effect on the film stability. The total electronic energy $A(N)$ of the system is computed from a sum of all of the occupied states below the Fermi level within the first surface Brillouin zone. The quantity relevant to stability against $N \rightarrow N \pm 1$ bifurcation is the energy difference defined as

$$\Delta(N) \equiv \frac{1}{2}[A(N+1) + A(N-1)] - A(N) \qquad (2)$$

which is just one-half of the discrete second derivative of $A(N)$. A large positive $\Delta(N)$ corresponds to a stable film. The results of our calculation (Fig. 3B) show that $N = 2$ and 5 are particularly stable, in agreement with the experiment.

The above calculation does not extend to $N = 1$, because $A(0)$ is ill-defined. Changes in geometry for a monolayer film must be accompanied by exposure of the substrate Fe surface, which has a much higher surface energy than Ag (*12*). Ag nominally wets an Fe surface based on this surface-tension consideration, and this probably accounts for the stability of the monolayer film.

The high stability for $N = 5$ can be understood in terms of the quantum-well state energies at the surface zone center. The energy spacings between quantum-well states are generally smooth, monotonic functions of N. As mentioned above, a film thickness of $N = 4$ yields a quantum-

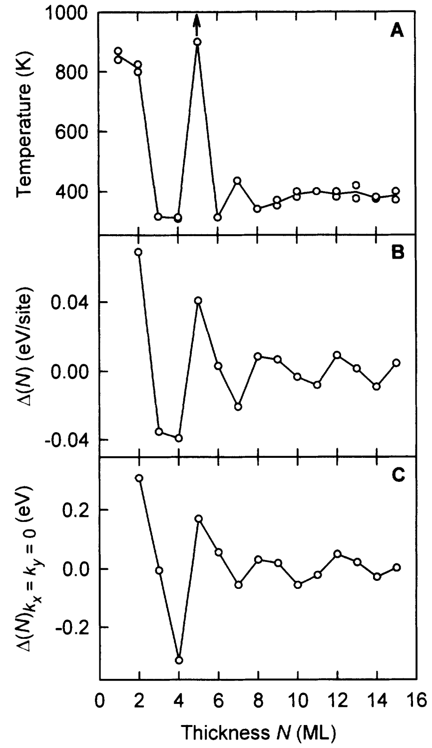

Fig. 3. (**A**) Temperatures at which films with an initial thickness of N begin to bifurcate. The $N = 5$ film is stable up to the highest temperature used in the experiment, and the arrow indicates that the data point represents a lower bound. (**B**) Calculated energy difference $\Delta(N) \equiv \frac{1}{2}[A(N+1) + A(N-1)] - A(N)$ against bifurcation as a function of N. (**C**) Results from the same calculation but without the summation over k_x and k_y.

well peak very close to the Fermi level at $E = 0$. Increasing the quantum-well width to $N = 5$ causes this state to drop below the Fermi level. This becomes the topmost-occupied quantum-well state for $N = 5$, and it is unusually deep below the Fermi level relative to the other cases (see Fig. 1). The whole subband has, on average, a lower energy, leading to an overall lower energy for the system. This argument suggests that film stability is mainly determined by the quantum-well state energies at the surface zone center. To verify this, Eq. 2 is reevaluated without summing over k_x and k_y. Indeed, the results (Fig. 3C) show the same general pattern for stability; namely, $N = 2$ and 5 are highly stable. Summing over a limited circle in k_x and k_y space leads to the same conclusion. A corollary is that detailed band structure features including the (111) neck do not play an important role.

The dominant issue for film stability is thus the phase-shift function Φ, which directly affects the quantum-well energies. In the present case, photoemission measurements provide an accurate determination of Φ, which is critical to the quantitative analysis presented above. Simple models based on one-dimensional potential wells, adopted in previous studies of metal films on semiconductors (*5*), generally do not lead to accurate quantum-well levels and are thus unable to explain our results quantitatively. Other effects that are important for metal-semiconductor interfaces, including an interface capacitor term (*5*), are found to be unimportant in the present case of a metal-metal interface. Using atomically uniform films in our experiment, questions regarding multiple steps do not arise, and the issue of stability reduces to a simple $N \rightarrow N \pm 1$ bifurcation as the first step toward roughening. For rough or nonuniform films, the situation can be far more complex, as there can be a multitude of paths for film-morphology evolution, including, for example, step bunching and pyramid formation.

A general strategy for stability engineering in nanostructures is thus to tailor the geometry to minimize the energies of the occupied states relative to the Fermi level. This is similar to the issue of stability for clusters (*13*) and nanowires (*14*), which prefer structures with a closed electronic shell. For Ag films considered here, adding one atomic layer generally leads to the addition of a partially occupied subband. The $N = 5$ case is an exception. Without a new subband below the Fermi level, it resembles a shell-closing point. Its topmost subband below the Fermi level is relatively deep, leading to a highly stable film. In going from clusters to wires and to films, the dimensionality of confinement is reduced from three to two and then to one. For films, the energy continuum in the other two dimensions tends to diminish this shell-closing effect. Nevertheless, quantum variations in stability remain an important effect, as shown in this study.

References and Notes

1. *Nanotechnology Research Directions*, Workshop Report by the Interagency Working Group on Nanoscience, Engineering and Technology, Committee on Technology, National Science and Technology Council for the Executive Office of the President of the United States of America, M. C. Roco, S. Williams, P. Alivisatos, Eds. (September 1999), available at www.sc.doe.gov/production/bes/iwgn.research.directions/welcome.htm.
2. J. J. Paggel, T. Miller, T.-C. Chiang, *Phys. Rev. Lett.* **81**, 5632 (1998).
3. A. R. Smith, K.-J. Chao, Q. Niu, C. K. Shih, *Science*, **273**, 226 (1996).
4. D. A. Evans, M. Alonso, R. Cimino, K. Horn, *Surf. Sci.* **376**, 1 (1997).
5. Z. Zhang, Q. Niu, C. K. Shih, *Phys. Rev. Lett.* **80**, 5381 (1998).
6. E. Tosatti, S. Prestipino, *Science* **289**, 561 (2000).
7. Y. Kondo, K. Takayanagi, *Science* **289**, 606 (2000).
8. J. J. Paggel, T. Miller, T.-C. Chiang *Science* **283**, 1709 (1999).
9. ———, *Phys. Rev. B* **61**, 1804 (2000).
10. T.-C. Chiang, *Surf. Sci. Rep.* **39**, 181 (2000).
11. N. V. Smith, L. F. Mattheiss, *Phys. Rev. B* **9**, 1341 (1974).
12. V. K. Kumikov, Kh. B. Khokonov, *J. Appl. Phys.* **54**, 1346 (1983).
13. W. D. Knight *et al.*, *Phys. Rev. Lett.* **52**, 2141 (1984).
14. A. I. Yanson, I. K. Yanson, J. M. van Ruitenbeek, *Nature* **400**, 144 (1999).
15. Supported by the U.S. National Science Foundation (grants DMR-99-75470 and DMR-99-75182 to T.C.C) and the U.S. Department of Energy (grant DEFG02-97ER45632 to M.Y.C.). We acknowledge the Petroleum Research Fund, administered by the American Chemical Society, and the U.S. Department of Energy, Division of Materials Sciences (grant DEFG02-96ER45439), for partial support of the synchrotron beamline operation and the central facilities of the Materials Research Laboratory. The Synchrotron Radiation Center of the University of Wisconsin–Madison, where the experiment was done, is supported by the U.S. National Science Foundation (grant DMR-00-84402).

24 January 2001; accepted 19 March 2001

Proposed Square Spiral Microfabrication Architecture for Large Three-Dimensional Photonic Band Gap Crystals

Ovidiu Toader and Sajeev John

We present a blueprint for a three-dimensional photonic band gap (PBG) material that is amenable to large-scale microfabrication on the optical scale using glancing angle deposition methods. The proposed chiral crystal consists of square spiral posts on a tetragonal lattice. In the case of silicon posts in air (direct structure), the full PBG can be as large as 15% of the gap center frequency, whereas for air posts in a silicon background (inverted structure) the maximum PBG is 24% of the center frequency. This PBG occurs between the fourth and fifth bands of the photon dispersion relation and is very robust to variations (disorder) in the geometrical parameters of the crystal.

Photonic band gap (*1, 2*) materials are artificial dielectric crystals with a periodicity on the optical wavelength scale. Because of a confluence of macroscopic (Bragg) and microscopic scattering resonances, these crystals can create a bound-state spectrum for electromagnetic waves with wavelengths comparable to the lattice constant. It is this